

The impact of South Pacific extratropical forcing on ENSO and comparisons with the North Pacific

Ruiqiang Ding · Jianping Li · Yu-heng Tseng

Received: 5 December 2013 / Accepted: 16 August 2014 / Published online: 31 August 2014
© Springer-Verlag Berlin Heidelberg 2014

Abstract Previous studies suggest that North Pacific extratropical atmospheric variability influences ENSO via the seasonal footprinting mechanism (SFM). This study confirms that quadrupole sea surface temperature (SST) variability in the extratropical South Pacific triggered by mid-latitude South Pacific atmospheric variability may also have an additional influence on ENSO. The response of the evolution of the ENSO-related zonal wind and SST anomalies in the tropics to the South Pacific extratropical forcing is consistent with the SFM hypothesis. That is, the Pacific–South American (PSA) pattern of the South Pacific extratropical sea level pressure (SLP) anomalies imparts an SST footprint (i.e., a quadrupole SST pattern) onto the ocean during austral summer. This SST footprint subsequently forces the zonal wind anomalies along the equator in the following austral winter that ultimately result in ENSO events during the following austral summer via ocean–atmosphere coupling in the tropics. The present study demonstrates that the influences of extratropical

atmospheric variability in the South Pacific and North Pacific on ENSO are different and relatively independent. It is possible that they may, together or separately, influence the occurrence of ENSO events, and the importance of the South Pacific forcing in initiating ENSO events is comparable with that of the North Pacific forcing. An empirical model was established to predict the Niño3.4 index based on the combined South Pacific and North Pacific signals, and results show that it can be used to produce skillful forecasts of the Niño3.4 index with a leading time of up to 1 year.

Keywords The Pacific–South American (PSA) pattern · ENSO · Quadrupole SST pattern

1 Introduction

Previous studies have suggested a physical connection between intrinsic atmospheric variability over the North Pacific in a particular boreal winter and ENSO in the following boreal winter (Vimont et al. 2001, 2003a, b; Alexander et al. 2010; Yu and Kim 2011). The so-called seasonal footprinting mechanism (SFM) has been proposed by Vimont et al. (2001, 2003a, b) to explain this connection. The SFM suggests that fluctuations in the wintertime North Pacific Oscillation (NPO) (Walker and Bliss 1932; Rogers 1981), the second leading mode of sea level pressure (SLP) variability over the North Pacific, initiate a sea surface temperature (SST) footprint onto the ocean via changes in the net surface heat flux. This SST footprint, which reaches a maximum in late boreal winter and early boreal spring, persists until boreal summer in the subtropics, where it can subsequently force the overlying atmosphere, resulting in zonal wind stress anomalies along the equator that

R. Ding · J. Li (✉)
State Key Laboratory of Numerical Modeling for Atmospheric Sciences and Geophysical Fluid Dynamics (LASG), Institute of Atmospheric Physics, Chinese Academy of Sciences, P.O. Box 9804, Beijing 100029, China
e-mail: ljp@bnu.edu.cn

J. Li
College of Global Change and Earth System Science (GCESS), Beijing Normal University, Beijing 100875, China

J. Li
Joint Center for Global Change Studies, Beijing 100875, China

Y. Tseng
Climate and Global Dynamics Division, NCAR, Boulder, CO, USA

are conducive to the initiation of an ENSO event during the following boreal winter.

Given that intrinsic atmospheric variability in the North Pacific exerts a forcing effect on ENSO, the question naturally arises as to whether intrinsic atmospheric variability in the South Pacific could also have an impact on ENSO. However, until now, the majority of studies have been devoted to the significant influence of ENSO on climate variability in the Southern Hemisphere, such as on the Antarctic Circumpolar Wave (ACW) or the Southern Annular Mode (SAM) (e.g., Carril and Navarra 2001; Kwok and Comiso 2002; Ribera and Mann 2003; Grassi et al. 2005; Fogt and Bromwich 2006; L'Heureux and Thompson 2006; Ding et al. 2012; Li et al. 2013a, b). In contrast, few investigations have examined Southern Hemisphere influences on ENSO. Vimont et al. (2003a) suggested that, unlike the Northern Hemisphere, Southern Hemisphere atmospheric variability has very little effect on the tropics in the CSIRO coupled general circulation models (CGCMs). They speculated that the SFM might be less effective in linking the Southern Hemisphere atmospheric variability and tropical variability for two reasons. First, SST anomalies (SSTAs) forced by patterns of Southern Hemisphere mid-latitude atmospheric variability do not extend to the deep tropics. Second, the atmosphere in the southern tropical Pacific is not as sensitive to SSTAs as is the atmosphere in the northern tropical Pacific, which could be due to the effect of colder mean SSTs in the southern tropics. However, despite this interpretation presented by Vimont et al. (2003a), there has been both observational and modeling evidence reported regarding Southern Hemisphere influences on ENSO. This evidence includes: the influence of the ACW on ENSO (Simmonds and Jacka 1995; White and Peterson 1996; Yuan and Martinson 2000; White and Annis 2004); the forcing of subtropical dipole SST variability in both the Southern Indian and Atlantic Oceans on ENSO (Terray 2011); SSTAs in the southeastern tropical Pacific (Toniazzo 2010) and southwestern Pacific (Holbrook and Bindoff 1997); and a zonal SST dipole near the Ross and Bellingshausen Seas (Ballester et al. 2011). All of these factors have been identified as useful precursors to the onset of El Niño, etc.

Figure 1a shows the spatial pattern of the austral summer [November–April (NDJFMA)] averaged SLP anomalies regressed against the austral summer (NDJFMA-averaged) cold tongue index (CTI) during the following year in the Pacific. A pronounced NPO-like pattern over the North Pacific can be seen to precede ENSO by 1 year, which is consistent with the findings of Vimont et al. (2001, 2003a, b). In addition to the preceding signal over the North Pacific, we notice that a marked wave train from the mid-latitude southwestern Pacific to Argentina with three centers of SLP anomalies over the South Pacific also

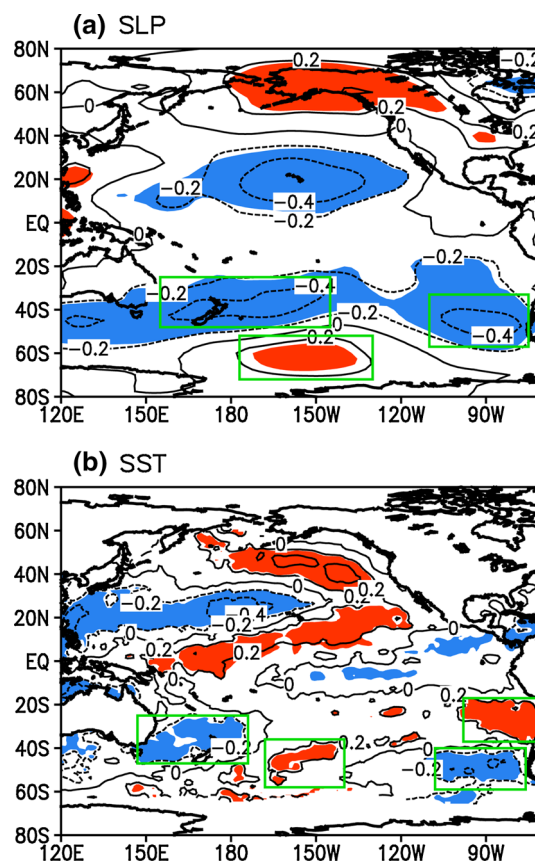


Fig. 1 Spatial pattern of the austral summer [November–April (NDJFMA)] averaged **a** SLP (mb) and **b** SST (°C) anomalies regressed against the austral summer (NDJFMA-averaged) cold tongue index (CTI) during the following year [the CTI is defined as SST averaged over (180°–90°W, 6°S–6°N) and is a commonly used index of ENSO variability]. Positive (red) and negative (blue) SLP and SST anomalies, with regression coefficients significant at the 0.05 level, are shaded. In (a), three green boxes [positive regression box: (177°–130°W, 72°–52°S); negative regression boxes: (155°E–145°W, 48°–25°S) and (110°–75°W, 57°–33°S)] indicate the locations of three action centers of the PSA, respectively. In (b), four green boxes [from left to right: (142°E–179°W, 47°–25°S); (173°–145°W, 58°–36°S); (113°–81°W, 59°–40°S); and (103°–76°W, 37°–17°S)] define the locations of the four poles of the SPQ

precedes ENSO by 1 year. This SLP pattern resembles the first Pacific–South American (PSA) pattern shown in Fig. 1 of Mo (2000). Mo (2000) reported that the first empirical orthogonal function (EOF) mode of the Southern Hemisphere winter season [June–August (JJA)] 500 hPa geopotential height is the Antarctic Oscillation (AAO) pattern (Gong and Wang 1999; Thompson and Wallace 2000), and the second and third EOF modes are the PSA patterns, the phases of which are nearly in quadrature with each other. Furthermore, Karoly (1989) showed that the first PSA pattern is dominant in the Southern Hemisphere during the developing phase of ENSO (JJA). Jin and Kirtman (2009) reported that the PSA pattern in the extratropical Southern

Hemisphere leads the peak phase of ENSO by one season. These studies have shown a close linkage between the PSA and ENSO. However, a detailed analysis of how and to what extent the PSA pattern affects ENSO, as well as the relative contributions of the South and North Pacific extratropical forcings to ENSO, is still lacking.

Motivated by the lead–lag relationship in Fig. 1a, and the pioneering work of Vimont et al. (2003a, b), this study aims to establish the existence of intrinsic atmospheric variability over the extratropical South Pacific that may act as the effective stochastic forcing of ENSO. Specific questions of interest include: Can the PSA, like the NPO, initiate an SST footprint onto the ocean? If so, how does this SST footprint affect ENSO? Does the SFM play an important role in linking the PSA to ENSO? Are there any differences between the influences of the South and North Pacific on ENSO?

The remainder of this manuscript is organized as follows. Data and methodology are described in Sect. 2. Section 3 investigates the effect of the PSA pattern on the ocean. Section 4 explores the link between the PSA and ENSO, and the mechanism by which the PSA forces the onset of ENSO events. A further discussion comparing the influence of the South and North Pacific on ENSO is given in Sect. 5. Finally, Sect. 6 summarizes and discusses the major results.

2 Data and methods

2.1 Observational data

The SST dataset used in this study was the Hadley Center Sea Ice and SST dataset (HadISST) on a $1^\circ \times 1^\circ$ spatial grid for the period 1950–2011 (Rayner et al. 2006). For subsurface ocean temperature information, we used the Simple Ocean Data Assimilation (SODA) version 2.2.4 for the period 1950–2008 (Carton and Giese 2008). The SODA dataset has 40 vertical levels unevenly distributed from 5 to 5,375 m and cover the global oceans from 75.25°S to 89.25°N with a horizontal resolution of $0.5^\circ \times 0.5^\circ$. The ocean mixed layer depth (MLD) is calculated in SODA using the criterion of an absolute temperature difference of 0.2°C from the surface (Montegut et al. 2004). For the analysis of atmospheric circulation, we used the National Centers for Environmental Prediction–National Center for Atmospheric Research (NCEP–NCAR) atmospheric reanalysis on a $2.5^\circ \times 2.5^\circ$ grid (Kalnay et al. 1996). The NCEP–NCAR reanalysis used in this study includes SLP, surface winds, and surface heat flux fields for the period 1950–2011. In this paper, the monthly anomalies were calculated by subtracting the climatological mean annual cycle.

2.2 Effective number of degrees of freedom

To calculate the correlation between the monthly data of two variables X and Y , the effective sample size N^* was estimated using the modified Chelton method (Pyper and Peterman 1998; Li et al. 2012, 2013a, b). The N^* can be obtained from the theoretical approximation:

$$N^* \approx \frac{N}{1 + 2 \sum_{i=1}^N \frac{N-i}{N} R_X(i) R_Y(i)}, \quad (1)$$

where N is the number of available time steps and $R_X(i)$ and $R_Y(i)$ are the autocorrelations of the two sampled time series $X(i)$ and $Y(i)$ ($i = 1, \dots, N$), respectively.

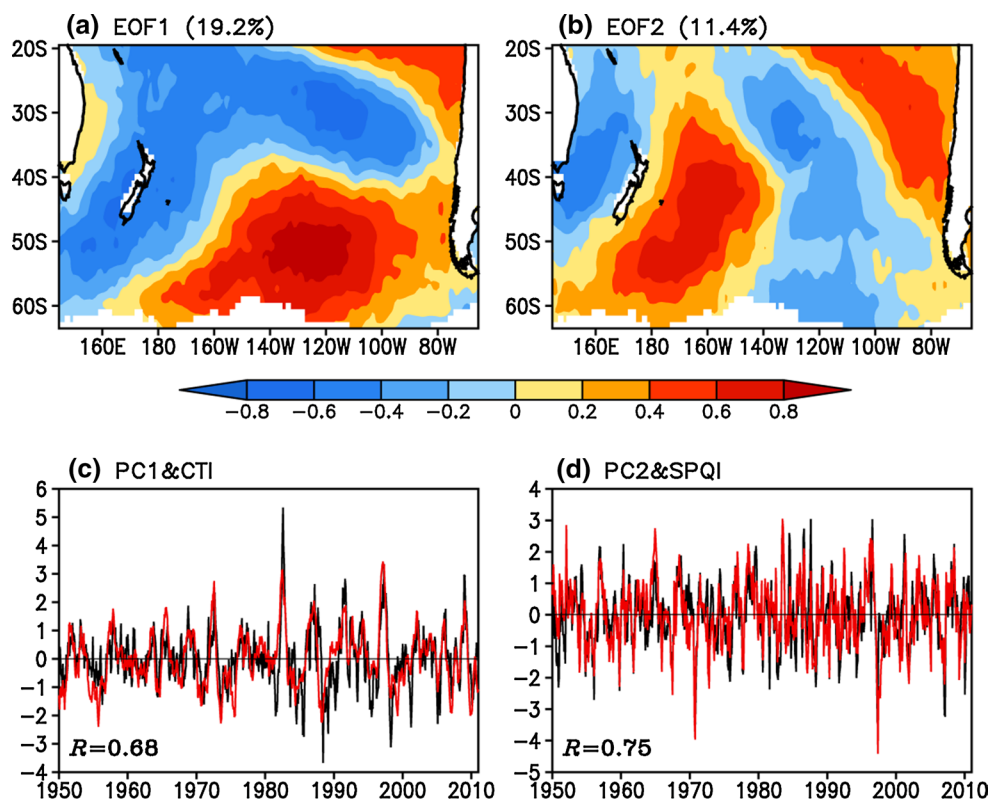
3 The effect of the PSA forcing on the ocean

Previous studies have demonstrated in detail how NPO-like atmospheric variability induces changes in surface heat fluxes, which, in turn, generate a dipole SST pattern in the North Pacific poleward of 20°N (Vimont et al. 2003a, b; Alexander et al. 2010; Yu and Kim 2011). This dipole SST pattern represents the second dominant mode (EOF2) of the North Pacific (poleward of 20°N) SST variability independent of the Pacific Decadal Oscillation (PDO), referred to as the Victoria mode (VM) (Bond et al. 2003). Ding et al. (2014, manuscript submitted to *J. Geophys. Res.*, hereafter DLTS) suggest that the VM may act as an effective pathway for NPO-like atmospheric variability to drive ENSO variability via the SFM. From the point of view of the whole Pacific Ocean, the results in Fig. 1a also show a close connection between the austral summer PSA and ENSO during the following austral summer. Whether the PSA can initiate an SST footprint onto the ocean like the NPO, which may play an important role in linking the austral summer PSA with ENSO in the following austral summer, will now be considered. In this section, we examine in detail the response of the South Pacific SST variability to the PSA atmospheric forcing.

As shown earlier in Fig. 1a, the austral summer SLP pattern associated with ENSO during the following austral summer exhibits a wave train structure from the mid-latitude South Pacific to Argentina with large amplitudes in the Pacific–South America sector. This SLP pattern is herein referred to as the PSA (Mo and Higgins 1998; Mo 2000). The PSA index (PSAI) is defined as the difference between the normalized SLP anomalies averaged over the positive center and the sum of the normalized SLP anomalies averaged over two negative centers, as shown in Fig. 1a.

In addition to the significant SLP anomalies in the North and South Pacific that precede ENSO by 1 year in Fig. 1a, we note that there also exist significant SSTA signals in

Fig. 2 Spatial patterns of **a** EOF1 and **b** EOF2 of the monthly normalized SSTA field over the South Pacific poleward of 20°S for the period 1950–2011 (after removing the monthly mean global average SSTA). **c** Time series of the PC1 (black line) overlaid with the monthly CTI (red line). **d** Time series of the PC2 (black line) overlaid with the monthly SPQI (red line). In (c) and (d), the correlation between two time series is given in the lower left corner



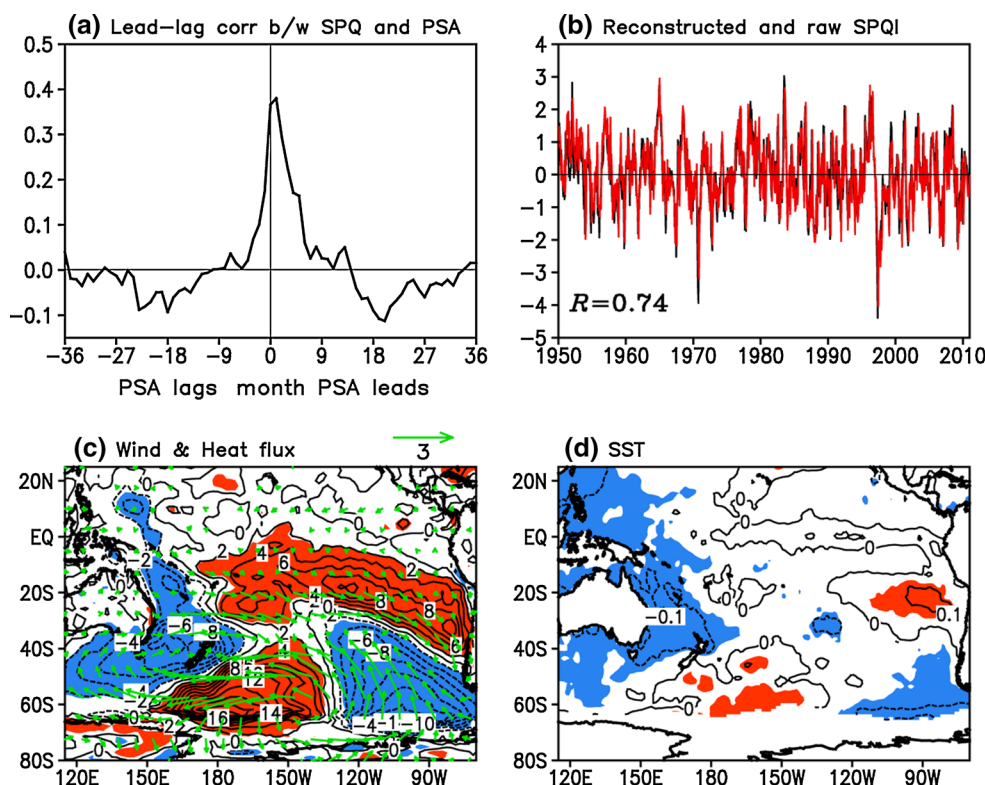
the North and South Pacific that precede ENSO by 1 year (Fig. 1b). The significant SSTA signal in the North Pacific exhibits a tripole-like pattern (consisting of a dipole SSTA pattern of the VM in the North Pacific poleward of 20°N and a subtropical pole of positive SSTA located in the central–eastern North Pacific, both of which are forced by the NPO), which has been noted in previous studies (Vimont et al. 2003a, b; Alexander et al. 2010; Yu and Kim 2011). The significant SSTA signal in the South Pacific exhibits a quadrupole-like structure, characterized by negative SSTAs in the Tasman Sea off the southeast coast of Australia, positive SSTAs near the Ross Sea, negative SSTAs near the Bellingshausen Sea, and positive SSTAs extending westward from the west coast of South America to near 100°W. For brevity, we hereafter refer to this South Pacific quadrupole SST pattern as the SPQ. To quantitatively depict the SPQ signal that precedes ENSO, a simple SPQ index (SPQI) was defined as the difference between the sum of the normalized SSTAs averaged within the two boxes where the regressed SSTAs are positive, and the sum of the normalized SSTAs averaged within the other two boxes where the regressed SSTAs are negative. The boxes that were used to construct the SPQI are indicated in Fig. 1b.

The first two leading EOF modes of the monthly normalized SSTA field in the South Pacific poleward of 20°S for the period 1950–2011 (after removing the monthly mean global average SSTA) are presented in Fig. 2a, b,

respectively. EOF1 and EOF2 account for 19.2 and 11.4 % of the extratropical South Pacific SST variability, respectively, and are well separated from the remaining EOFs, based on the criteria of North et al. (1982). The EOF1 pattern captures the large-scale horseshoe-like SSTA pattern in the extratropical South Pacific during the developing and mature phases of El Niño event (Kidson and Renwick 2002; Kwok and Comiso 2002; Terray 2011). The PC1 time series associated with EOF1 and CTI exhibit remarkably similar variability (with a correlation of 0.68) (Fig. 2c). EOF2 captures a zonal quadrupole SSTA pattern in the extratropical South Pacific and resembles the quadrupole-like SST pattern preceding ENSO by 1 year, as shown in Fig. 1b. The PC2 time series associated with EOF2 has a correlation of 0.75 with the SPQI (Fig. 2d). The strong correlation (>0.7) between the SPQI and the PC2 time series indicates the accuracy of the SPQI in representing the quadrupole SST mode in the extratropical South Pacific. These results indicate that, as with the VM that represents EOF2 of North Pacific (poleward of 20°N) SST variability, the SPQ represents EOF2 of South Pacific (poleward of 20°S) SST variability.

To explore the linkage between the PSA and SPQ, we show in Fig. 3a the lead–lag correlations between the monthly PSA and SPQ indices. The highest correlation ($R = 0.38$, significant at the 0.001 level) occurs when the PSA leads the SPQ by 1 month, indicating a significant

Fig. 3 **a** Lead–lag correlations between the raw monthly PSA and SPQ indices. **b** Observed (black line) and reconstructed (red line) SPQI using an AR1 model forced by the PSA. The correlation coefficient (R) between the monthly values of observed and reconstructed SPQ indices is given in the lower left corner. **c** Pacific surface wind (m s^{-1} ; vectors) and surface heat flux (W m^{-2} ; contours) anomalies regressed on the PSAI. **d** Pacific SSTAs ($^{\circ}\text{C}$; contours) regressed on the previous month’s PSAI. In (c) and (d), positive (red) and negative (blue) surface heat flux and SST anomalies, with regression coefficients significant at the 0.05 level, are shaded. In (c), only surface wind vectors significant at the 0.05 level are shown



influence of the atmosphere on the ocean. To quantify the oceanic response of the SPQ to atmospheric forcing, we follow the approach of Newman et al. (2003) and Schneider and Cornuelle (2005), and assume that the change of the monthly SPQ is governed by an autoregressive model of order 1 (AR1),

$$SPQ_t = \alpha \cdot PSA_{t-1} + \beta \cdot SPQ_{t-1} + \eta_t, \tag{2}$$

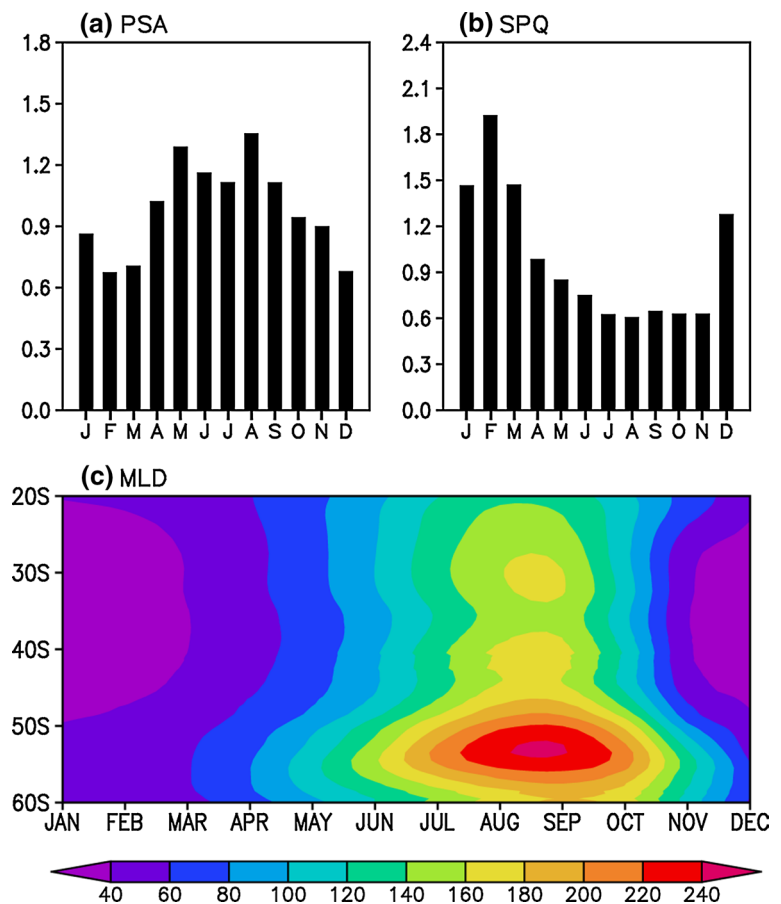
where the first and second terms on the right-hand side represent the PSA forcing index and the damping term, respectively, and η_t is uncorrelated noise. The coefficients $\alpha = 0.38$ and $\beta = 0.63$ were obtained from observations by regressing the SPQ against the previous month’s PSA, removing the PSA term, then regressing the residual against the previous month’s SPQ. The reconstructed monthly SPQI obtained from Eq. (2) and the raw monthly SPQI have a strong correlation ($R = 0.74$, significant at the 0.001 level) (Fig. 3b). This suggests that ~50 % of the SPQ variability is forced by the PSA atmospheric variability.

But why does the PSA induce a quadrupole SST pattern in the South Pacific? To address this question, we show in Fig. 3c, d the regression of surface wind and surface heat flux anomalies onto the PSAI, and SSTAs onto the previous month’s PSAI. The figures show that in the Tasman Sea, off the southeast coast of Australia, westerly wind anomalies associated with the PSA strengthen the climatological westerlies and increase the surface heat flux from ocean to atmosphere (i.e., negative surface heat flux anomalies),

which in turn generate an anomalously cool SST in the region. Conversely, in the mid-latitude South Pacific near the Ross Sea, easterly wind anomalies associated with the PSA weaken the climatological westerlies and decrease the surface heat flux from ocean to atmosphere (i.e., positive surface heat flux anomalies), which leads to an anomalously warm SST there. In the mid-latitude South Pacific near the Bellingshausen Sea, southeasterly wind anomalies associated with the PSA advect cool and dry air into the region to increase the surface heat flux from ocean to atmosphere, and consequently produce the negative SSTAs there. In the area extending westward from the west coast of South America to near the dateline, northwesterly wind anomalies associated with the PSA weaken the southeasterly trade winds and subsequently decrease the surface heat flux from ocean to atmosphere and also coastal upwelling, which tends to maintain an anomalously warm SST there. These results indicate that anomalous surface winds associated with the PSA can force a quadrupole-like pattern onto the surface heat flux anomalies, which in turn induces a quadrupole SST pattern.

Figure 4a, b show the seasonal variations in the standard deviations of the PSA and SPQ indices. The figure shows that the PSA attains maximum variance during May–September (MJJAS) (Fig. 4a), while the SPQ shows maximum variance during December–April (DJFMA) (Fig. 4b). This inconsistent seasonality of the SPQ and PSA is possibly due to the influence of the seasonal variation of the MLD in

Fig. 4 **a** Seasonal variations of the standard deviation of the PSAI. **b** Seasonal variations of the standard deviation of the SPQI. **c** Seasonal variations of the zonally averaged mixed layer depth (MLD; m) over 155°E–85°W



the extratropical South Pacific. The MLD in the extratropical South Pacific is deep during austral winter and shallow during austral summer (Fig. 4c), consistent with the seasonal variation of surface wind stress. The shallow MLD in the extratropical South Pacific tends to amplify the SPQ-related SST response to surface wind anomalies associated with the PSA, and therefore leads to the maximum variance of the SPQ during austral summer. This indicates that the PSA forced SST pattern in the extratropical South Pacific is sensitive to local seasonality, modulated by the seasonal variations of the MLD. These features of seasonal variations of the PSA and SPQ differ from those of the NPO and VM. DLTS show that both the strongest NPO and VM occur during boreal winter (JFM). A possible explanation for this difference may be that the NPO is strong enough during boreal winter to force a strong SST footprint onto the ocean with a deep mixed layer. According to DLTS, the NPO exhibits a remarkable seasonal variation, which is much stronger during boreal winter, but weaker during boreal summer. However, despite the fact that both the South and North Pacific atmospheric variability (corresponding to the PSA and NPO, respectively) peak in opposite seasons (JJA and JFM, respectively), the SST footprints

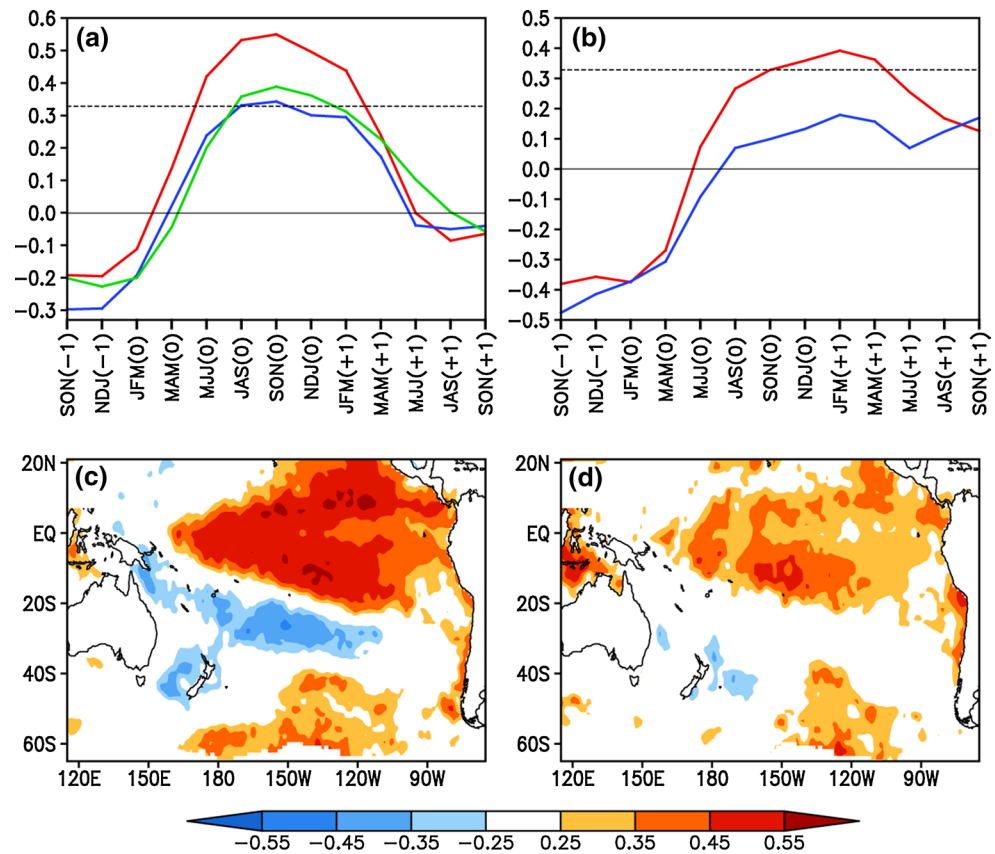
(corresponding to the SPQ and VM, respectively) forced by the atmospheric variability peak in the same season (JFM).

4 Establishing the PSA–SPQ–ENSO relationship

4.1 Relationships between the PSA/SPQ and ENSO

Section 3 established that the SPQ is an oceanic response to the atmospheric forcing of the PSA, but this response is modulated by the seasonal variations of the MLD. We now turn to the relationships between the PSA/SPQ and ENSO. Lead–lag correlations between the austral summer(0) (JFM-averaged) PSAI and 3-month averaged CTI, and between the austral summer(0) SPQI and 3-month averaged CTI, are shown in Fig. 5a. Hereafter, we denote the year in which the SPQ peaks in JFM as year 0 and the preceding and following years as year –1 and +1, respectively. For the SPQ, the peak correlation ($R = 0.55$) occurs during September–November(0) [SON(0)], lagging the peak of the SPQ during JFM(0) by 9 months. For the PSA, the peak correlation ($R = 0.34$) also occurs during SON(0). In comparison, for lead times of a few months to more than

Fig. 5 **a** Lead–lag correlations of the 3-month averaged CTI with the JFM(0)-averaged SPQI (red line), PSAI (blue line), and residual SPQI (green line) obtained by linearly removing the reconstructed JFM(0)-averaged SPQI based on the PSAI, as obtained from Eq. (2), from the original JFM(0)-averaged SPQI (–1: year prior to the SPQI; 0: year concurrent with the SPQI; +1: year following the SPQI). **b** Lead–lag correlations of the 3-month averaged CTI with the JJA(0)-averaged SPQI (red line) and PSAI (blue line). **c** Correlation maps of the JFM(0)-averaged SPQI with the following NDJ(0) SSTAs. **d** As for (c), but for the residual JFM(0)-averaged SPQI. In **a**, **b** the horizontal dashed line shows the 0.01 significance level. In **c**, **d** areas with correlation significant at the 0.05 level are shaded



a year, the SPQ shows stronger correlations with the CTI than does the PSA.

To further investigate the relationships between the SPQ and ENSO after removing the effect of the PSA, we examine the partial correlation between the CTI and residual SPQI obtained by linearly removing the reconstructed JFM(0)-averaged SPQI based on the PSAI, as obtained from Eq. (2), from the original JFM(0)-averaged SPQI (Fig. 5a). With the removal of the PSA effect, the peak correlation ($R = 0.39$) in SON(0) is lower than that obtained from the original SPQI. However, for lead times of a few months to more than a year, the residual SPQ still shows slightly stronger correlations with the CTI than does the PSA. Furthermore, a comparison between correlation maps of the original and residual SPQI during JFM(0) with the SSTAs during November(0)–January(+1) [NDJ(0)] indicates that with the PSA effect removed, correlations in most regions of the tropical Pacific are substantially reduced but a distinct El Niño pattern remains (Fig. 5c, d).

These results support the idea that the PSA may provide an important source of atmospheric forcing to excite the SPQ (i.e., the SST footprint); however, the SPQ, as an ocean bridge (or conduit) linking the extratropical atmospheric forcing of the South Pacific to ENSO, has its own variability independent of the PSA, and is more directly linked to ENSO than is the atmospheric forcing itself. Our

results are consistent with the SFM proposed by Vimont et al. (2001, 2003a, b). The SFM suggests that once the SST footprint is generated by the atmospheric variability, the SST footprint, rather than the atmospheric variability, is most effective at forcing ENSO. This suggests that the PSA, although it is weak during austral summer, can force a strong SST footprint (corresponding to a strong SPQ) during austral summer due to the role of a thin MLD; therefore, it may act as effective external forcing to trigger ENSO during the following austral summer through the SFM. In contrast, although the PSA peaks during austral winter, it can only force a weak SST footprint (corresponding to a weak SPQ) due to the role of a deep MLD; consequently, the PSA during austral winter is not effective in triggering ENSO through the SFM, and so has a relatively weak correlation with ENSO during the following austral summer (Fig. 5b).

Based on the above results, we may conclude that although the PSA in the South Pacific and NPO in the North Pacific peak in opposite seasons (JJA and JFM, respectively), their resulting SST footprints (corresponding to the SPQ and VM, respectively) peak in the same season (JFM). And it is these SST footprints, rather than the atmospheric variability, that subsequently play a major role in triggering ENSO during the following boreal winter, thereby leading to similar seasonal phase relationships

between the South or North Pacific extratropical forcing and ENSO. Consequently, both the South and North Pacific extratropical forcings during boreal winter tend to trigger ENSO during the following boreal winter.

In addition, it is important to point out that, in contrast to previous studies that have separately emphasized the important role of SSTAs in the southeastern tropical Pacific (Toniazzo 2010), SSTAs in the southwestern Pacific (Holbrook and Bindoff 1997), or a zonal SST dipole near the Ross and Bellingshausen Seas (Ballester et al. 2011) as a precursor to ENSO, the present study emphasizes that the SPQ, as a basin-scale mode of South Pacific SST variability, combines all of the roles of SSTAs in the southeastern tropical Pacific, the southwestern Pacific, and the Ross and Bellingshausen Seas, and therefore may act as a more effective precursor to ENSO.

4.2 Maximum covariance analysis (MCA) results

To further elucidate the lagged coupling relationship between the SPQ and ENSO, we followed Vimont et al. (2003a) and performed a maximum covariance analysis (MCA; also known as singular value decomposition (SVD); Bretherton et al. 1992) with the three pairs of variables for the period 1950–2011: austral summer(0) South Pacific extratropical SST, austral winter(0) South Pacific tropical surface zonal wind (UWND), and austral summer(+1) (10 months later than the extratropical SST data) tropical Pacific SST. Here, the terms austral summer(0), winter(0), and summer(+1) refer to the consecutive seasons over which extratropical SST (DJFMA), tropical surface zonal wind (MJJAS), and tropical SST [October–February (ONDJF)] are averaged, respectively. Figure 6 shows the spatial and temporal domains of the data used to generate the MCA-II [austral summer(0) South Pacific extratropical SST and austral winter(0) South Pacific tropical surface zonal wind], MCA-III [austral summer(0) South Pacific extratropical SST and austral summer(+1) tropical SST], and MCA-III1 [austral winter(0) South Pacific tropical surface zonal wind and austral summer(+1) tropical SST]. Prior to the analysis, the austral summer(0) CTI was linearly removed from the austral summer(0) extratropical SST, winter(0) tropical zonal wind, and summer(+1) tropical SST data, which were then standardized. According to Vimont et al. (2003a), the removal of the austral summer(0) CTI from the data ensures that the austral winter(0) tropical zonal wind and the austral summer(+1) tropical SST are independent of any ENSO variability that may have occurred during the preceding winter.

The statistical results from the MCAs, including the total squared covariance fraction explained by the leading MCA mode, and the correlation between the associated expansion coefficient time series, are shown in Fig. 6. The

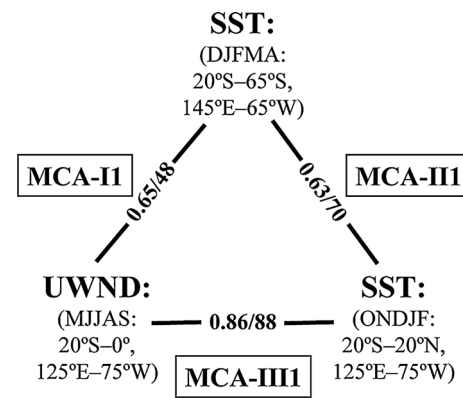


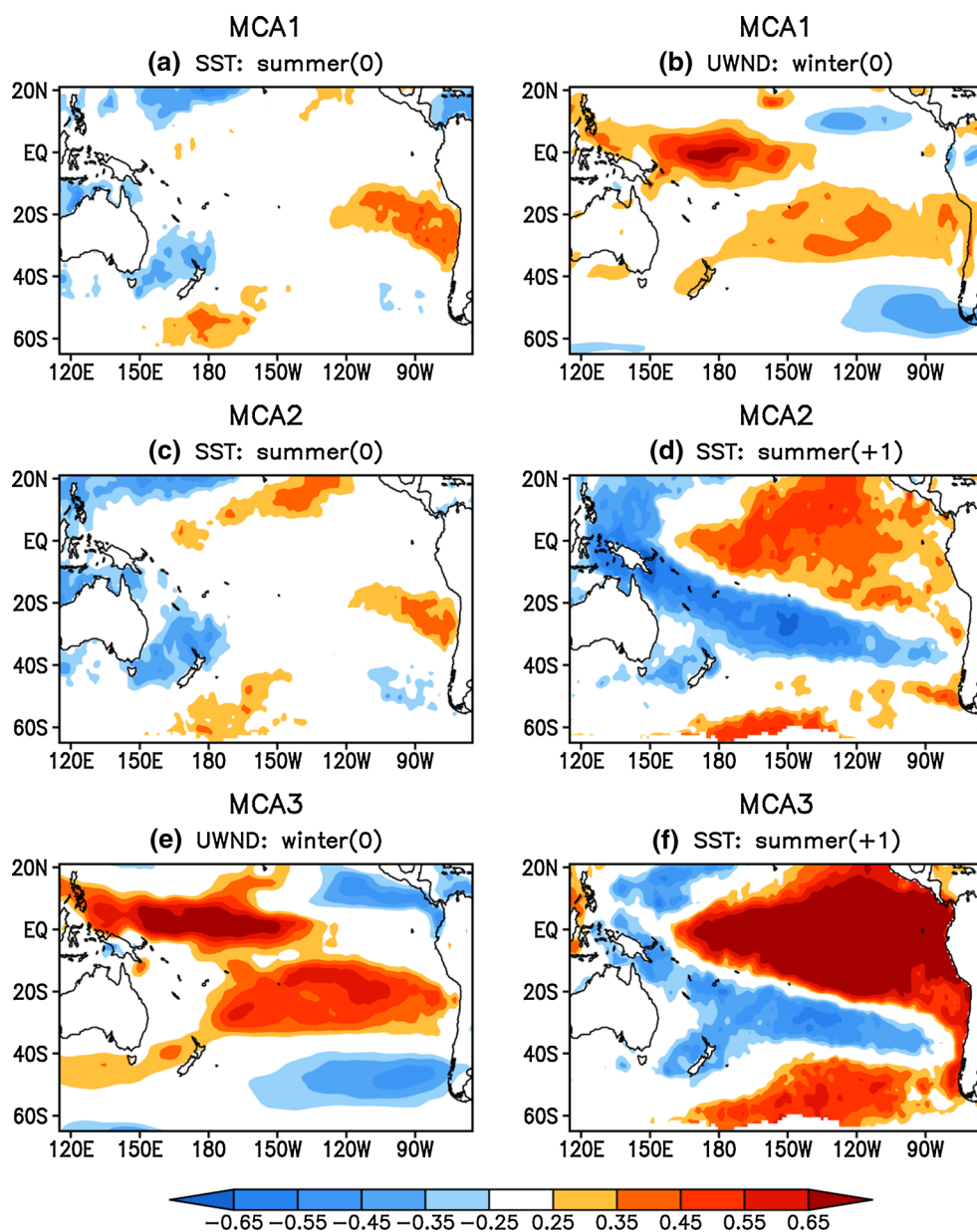
Fig. 6 Schematic representation of the data used in the three MCAs and summary statistics from the MCA. The summary statistics are in the following format: R/SCF , where R is the correlation between the associated expansion coefficient time series, and SCF is the total squared covariance fraction explained by the leading MCA mode

leading MCA mode explains about 48, 70, and 88 % of the total squared covariance between the two fields in MCA-II, MCA-III, and MCA-III1, respectively. The correlations between the expansion coefficient time series in the MCA-II, MCA-III, and MCA-III1 are 0.65, 0.63, and 0.86, respectively, and are all significant at the 0.001 level. These statistical results indicate that the three fields included in the MCAs are strongly coupled.

Figure 7a, b show the leading pair of heterogeneous patterns for MCA-II [austral summer(0) South Pacific extratropical SST and austral winter(0) South Pacific tropical surface zonal wind], which were generated by correlating the respective heterogeneous SST and zonal wind fields with the MCA-II leading normalized expansion coefficients. The austral summer(0) South Pacific SSTA pattern bears a resemblance to the regressed SSTA map in Fig. 1b, with a quadrupole-like SSTA distribution in the South Pacific poleward of 10°S. The southeastern pole of this quadrupole shows a very small anomaly, possibly indicating the limited importance of this pole in coupled patterns for MCA-II. During the following austral winter, the tropical surface zonal wind is characterized by positive anomalies in the western–central tropical Pacific extending from about 10°N to 15°S. These coupled patterns from MCA-II suggest that a quadrupole SSTA pattern in austral summer will be followed by the anomalous westerlies in the western–central tropical Pacific during the following austral winter.

Results from MCA-III1 [austral summer(0) South Pacific extratropical SST and austral summer(+1) tropical SST] show that, like the results from MCA-II, the austral summer(0) South Pacific SSTA map closely resembles the regressed SSTA map in Fig. 1b, exhibiting a quadrupole SSTA pattern in the South Pacific poleward of 10°S (Fig. 7c, d). During the following austral summer, the

Fig. 7 Spatial properties of leading heterogeneous patterns for the three separate MCA sets described in Fig. 6: **a, b** austral summer(0) SST and austral winter(0) surface zonal wind, respectively, from MCA1; **c, d** austral summer(0) SST and austral summer(+1) SST, respectively, from MCA2; **e, f** austral winter(0) surface zonal wind and austral summer(+1) SST, respectively, from MCA3. Leading heterogeneous patterns are shown as correlation maps of the respective heterogeneous fields onto the MCA leading normalized expansion coefficients. Areas with correlation significant at the 0.05 level are shaded

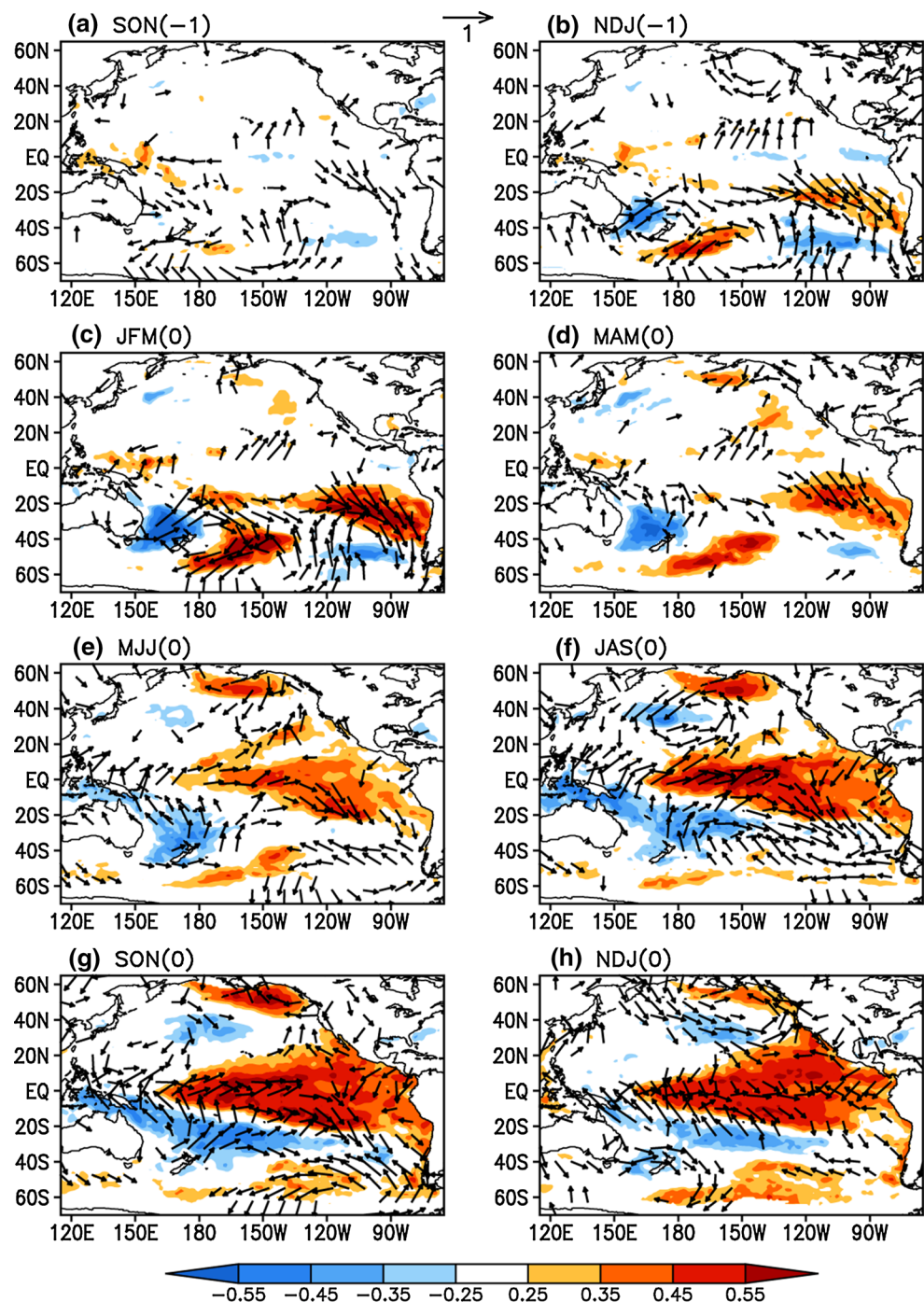


Pacific SST is dominated by positive anomalies in the eastern tropical Pacific and negative anomalies in the western tropical Pacific. These coupled patterns from MCA-III suggest that a strong SPQ in austral summer will be followed by a strong ENSO event during the following austral summer. This result agrees with the conclusions from Fig. 1b, and further confirms the strong lagged coupling relationship between the SPQ and ENSO.

Results from MCA-III1 capture the strongly coupled patterns between austral winter(0) tropical surface zonal wind and austral summer(+1) tropical SST, which are dominated by the development and mature stage of ENSO (Harrison and Larkin 1998). The zonal wind map from

MCA-III1 closely resembles the zonal wind map from MCA-II. The zonal wind time series from MCA-III1 and MCA-II have a correlation of 0.97 (significant at the 0.001 level), indicating that the South Pacific quadrupole-like SSTA distribution during austral summer(0) may lead to the zonal wind pattern seen in Fig. 7e. These MCA results from the South Pacific are similar to those from the North Pacific obtained by Vimont et al. (2003a), suggesting that, like the North Pacific forcing (i.e., the NPO/VM), the South Pacific forcing (i.e., the PSA/SPQ) during austral summer is followed by anomalous zonal wind stress along the equator during austral winter that is conducive to the initiation of an ENSO event during the following austral summer.

Fig. 8 Correlation maps of the JFM(0)-averaged SPQI with the 3-month averaged SST (*shaded*) and surface wind (vectors) anomalies for SON(-1) and NDJ(-1) preceding the SPQI, JFM(0) concurrent with the SPQI, and several lead times [MAM(0), MJJ(0), JAS(0), SON(0), NDJ(0)] for the period 1950–2011. Positive (*red*) and negative (*blue*) SSTAs, with the correlation coefficients significant at the 0.05 level, are shaded. Only surface wind vectors significant at the 0.05 level are shown

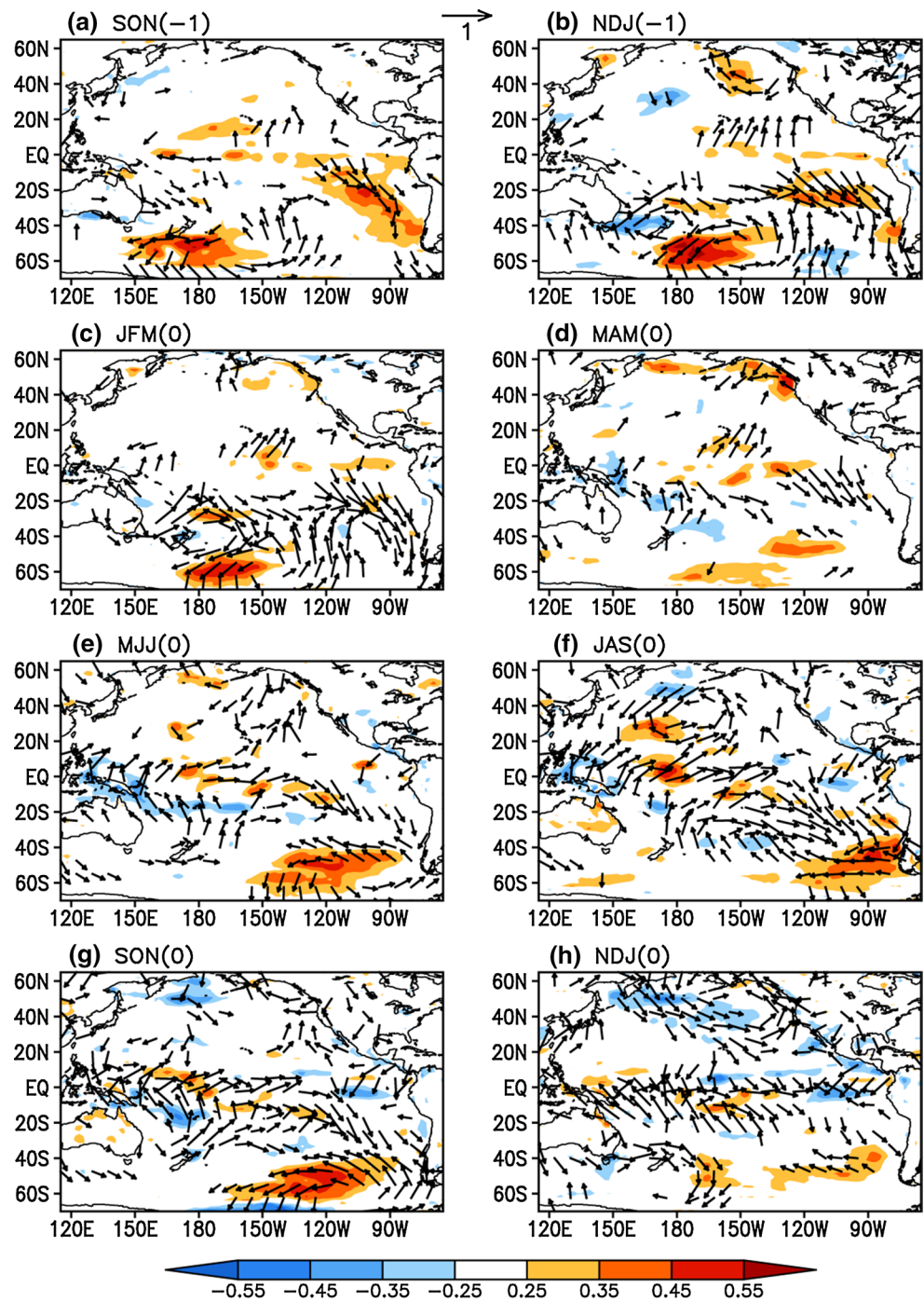


4.3 Mechanism linking the SPQ to ENSO

The above results demonstrate a significant lead-lag relationship between variability in the SPQ and ENSO. We now investigate the effect of the SPQ on ENSO by examining the spatial patterns of the 3-month averaged SST and surface wind anomalies correlated with the JFM(0)-averaged SPQI for a range of lead-lag times (Fig. 8). During SON(-1), about 4 months before the SPQ peaks,

significant positive SSTAs occur in the western tropical Pacific (Fig. 8a). At the same time, an anomalous circulation resembling the PSA develops in the mid-latitude South Pacific, consistent with changes in surface wind anomalies. The results suggest that anomalous warm SSTs in the western tropical Pacific may play an important role in developing the PSA. Our results are consistent with Ballester et al. (2011), who found that a warm SST anomaly in the western tropical Pacific generates an anomalous wave train

Fig. 9 As in Fig. 8, but for the 3-month averaged latent heat flux (LF) (*shaded*) and surface wind (*vectors*) anomalies correlated with the JFM(0)-averaged SPQI. For LF, downward flux that warms the ocean is defined as positive

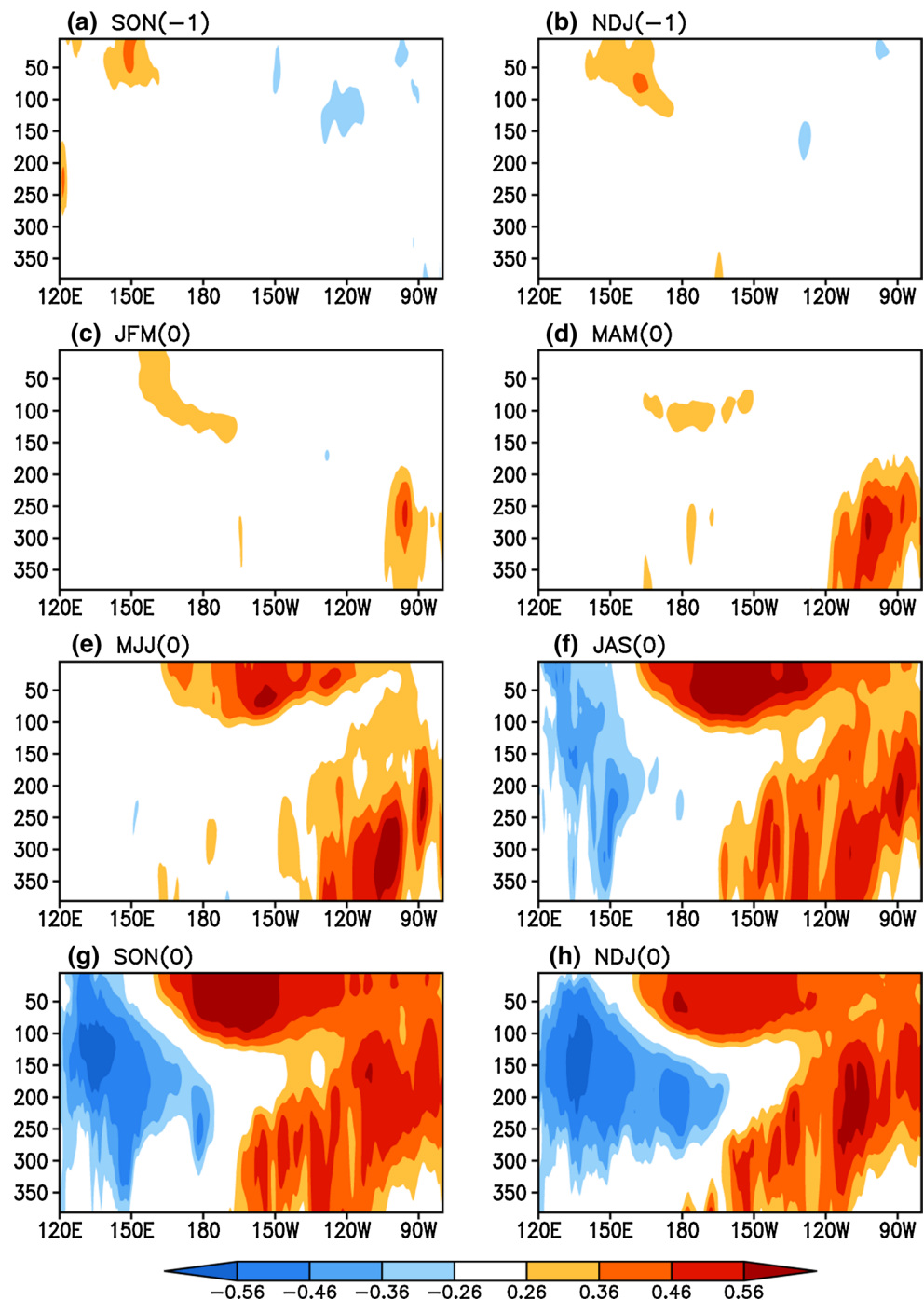


extending eastward and poleward in the Southern Hemisphere, which in turn produces a zonal SST dipole near the Ross and Bellingshausen Seas.

The strengthened PSA can then force a quadrupole-like SSTA pattern in the South Pacific via changes in the latent heat flux (LF) (Fig. 9a, b). During NDJ(-1), about 2 months before the SPQ peaks, a quadrupole-like SSTA pattern can be seen in the South Pacific south of 20°S (Fig. 8b). A few months after the SPQ peaks, in response to anomalous

southeasterlies associated with the SPQ, the southeasterly trade winds strengthen and subsequently enhance the upward LF (Fig. 9d, e), cooling the ocean along the north coast of Australia and leading to a positive wind–evaporation–SST (WES) feedback there (Xie and Philander 1994). This thermodynamic coupling results in northwestward development of negative SSTAs off the east coast of Australia and an associated equatorward shift in the surface zonal wind anomalies (Fig. 8e). The westerly component of

Fig. 10 Correlation maps of the JFM(0)-averaged SPQI with the 3-month averaged ocean subsurface temperature anomalies at different depths in meters averaged over 5°S–5°N for SON(–1) and NDJ(–1) preceding the SPQI, JFM(0) concurrent with the SPQI, and several lead times [MAM(0), MJJ(0), JAS(0), SON(0), NDJ(0)] for the period 1950–2008. Areas with the correlation coefficients significant at the 0.05 level are shaded



the anomalous surface winds along the equator favors the development of positive SSTA in the central–eastern equatorial Pacific (Fig. 8f). In addition, during MAM(0) and MJJ(0), in response to anomalous northwesterlies associated with the SPQ, the southeasterly trade winds weaken and subsequently reduce the upward LF (Fig. 9d, e), warming the ocean in the tropical southeastern Pacific and therefore leading to a positive WES feedback. This positive WES feedback leads to northwestward development

of positive SSTAs along the west coast of South America, strengthening the warming in the central–eastern equatorial Pacific (Fig. 8e). The warming in the central–eastern equatorial Pacific enhances the zonal SST gradient across the western–central equatorial Pacific (also across the eastern–central equatorial Pacific), which in turn amplifies the anomalous westerlies in the western equatorial Pacific and forces the anomalous easterlies in the eastern equatorial Pacific (Fig. 8f). The anomalous westerlies in the western

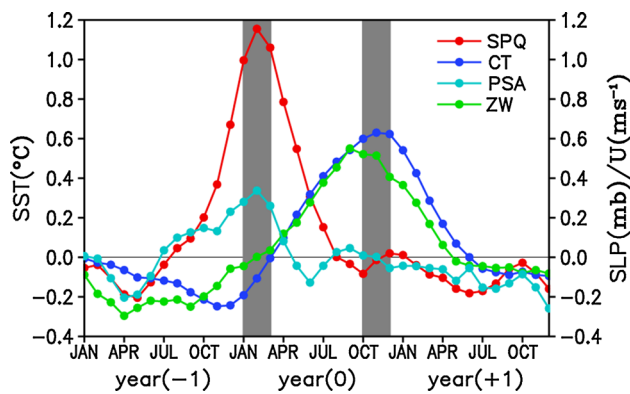


Fig. 11 Lead-lag regression coefficients of the 3-month running mean SPQI, CTI (scale on the left y-axis), area-averaged surface zonal wind (ZW) anomalies over the western-central equatorial Pacific (140°E – 170°W , 5°S – 5°N), and PSAI (scale on the right y-axis) on the austral summer(0) (JFM-averaged) SPQI. Areas shaded in gray denote the peak phases of the SPQ and ENSO. The year in which the SPQ peaks in JFM is denoted as year(0), and the preceding and following years as year(-1) and year(+1), respectively

Pacific (easterlies in the eastern Pacific) may excite downwelling equatorial Kelvin (Rossby) waves, which deepens the thermocline from the central to eastern tropical Pacific and thus increase the warming there (Fig. 10f). During SON(0), the warming in the central-eastern Pacific is further strengthened due to the arrival of downwelling equatorial Kelvin waves from the west and Rossby waves from the east (Fig. 10g). During NDJ(0), about 9 months after the SPQ peaks, a warming pattern is well developed in the eastern equatorial Pacific (Fig. 8h).

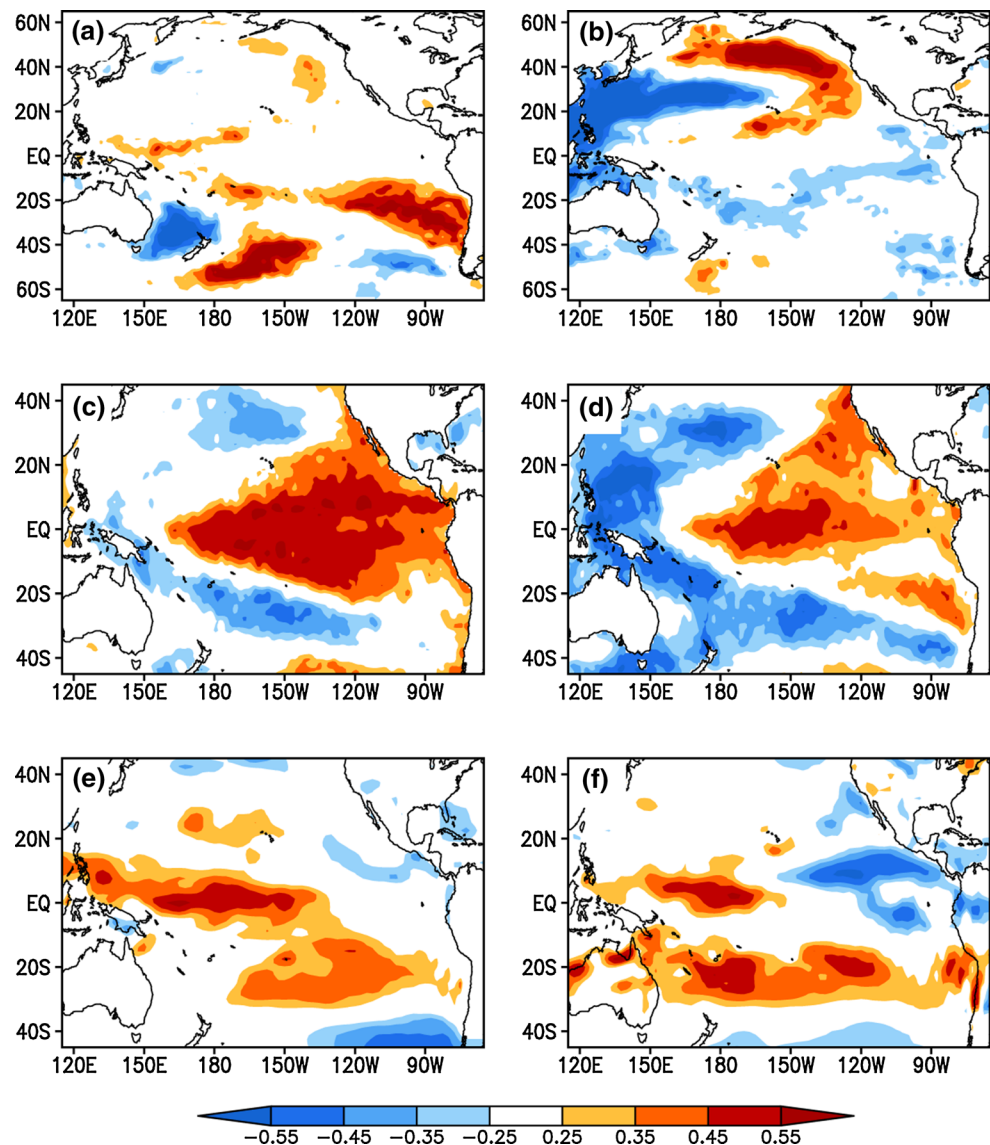
Figure 11 shows the lead-lag regression coefficients of the 3-month running mean PSAI, SPQI, area-averaged surface zonal wind anomalies over the western-central equatorial Pacific (140°E – 170°W , 5°S – 5°N), and CTI on the JFM(0)-averaged SPQI. As expected, the SPQ is strongest during austral summer(0), when it is regressed on itself. At the same time the PSA has a relatively weak peak during austral summer(0). This in-phase relationship between the PSA and SPQ suggests that the strongest SPQ during austral summer(0) may be an oceanic response to the forcing of the austral summer(0) PSA. The SSTAs associated with the SPQ (mainly its related subtropical portion) persist until austral winter(0) and extend into the tropics, which can subsequently force the zonal wind anomalies along the equator that favor the development of ENSO events. Note that CTI is relatively weak during austral summer(0), intensifies in phase with the zonal wind anomalies along the equator during austral winter(0), and peaks during OND(0), about 9 months after the peak of the SPQ. These phase relationships between the PSA, SPQ, zonal wind anomalies along the equator, and CTI are consistent with the SFM hypothesis proposed by Vimont et al. (2001, 2003a, b) that during

austral summer, South Pacific extratropical SLP variability [with a spatial structure that closely resembles the observed so-called PSA] imparts an SST footprint (i.e., a quadrupole SST pattern) onto the ocean. This SST footprint (mainly its related subtropical portion) then persists until austral winter and extends into the tropics, which can subsequently force the zonal wind anomalies along the equator that ultimately result in a strong ENSO event during the following austral summer via ocean-atmosphere coupling in the tropics.

5 Comparisons of the South and North Pacific influences

Recent studies have reported two different types of El Niño events. Kao and Yu (2009) refer to the new type of El Niño as the Central Pacific warming (CPW) El Niño, which exhibits maximum positive SSTAs in the central tropical Pacific, rather than the eastern tropical Pacific, as seen during conventional El Niño episodes. Different terms have also been used to describe the CPW El Niño, including the Date Line El Niño (Larkin and Harrison 2005), El Niño Modoki (Ashok et al. 2007), and warm-pool El Niño (Kug et al. 2009). Figure 12a–d show the boreal winter(0) (DJFMA-averaged) and winter(+1) (ONDJF-averaged) Pacific SSTAs correlated with the boreal winter(0) SPQ and VM indices, respectively. The figure demonstrates that both the SPQ and VM events in boreal winter are closely linked to an El Niño-like pattern in the tropical Pacific of the following boreal winter. In comparison, the center of the VM-related warming is located mainly in the central equatorial Pacific, with an SSTA pattern closely resembling the CPW El Niño, while the center of the SPQ-related warming is located in a larger domain covering almost the entire central-eastern tropical Pacific, with an SSTA pattern closely resembling the conventional El Niño. DLTS show that the VM can induce the CPW El Niño as well as the conventional El Niño, but it tends to be more conducive to the initialization of the CPW El Niño than the conventional El Niño. They show that the initial warming associated with the VM is located in the subtropical central-eastern North Pacific (see also Fig. 12b), and extends southwestward toward the central equatorial Pacific through a positive WES feedback process in boreal summer. The warming in the central equatorial Pacific then forces the anomalous westerlies in the western-central equatorial Pacific and the anomalous easterlies in the eastern-central equatorial Pacific, causing convergence in the central equatorial Pacific and in turn strengthening the warming there. This warming is sustained and trapped in the central equatorial Pacific by an active ocean-atmosphere feedback until the following boreal winter, finally establishing a CPW-like El Niño pattern in the tropical Pacific. In contrast, the present

Fig. 12 *Left: a* Boreal winter(0) SST, *c* winter(+1) SST, and *e* summer(0) surface zonal wind anomalies correlated with the boreal winter(0) SPQI. *Right: b* Boreal winter(0) SST, *d* winter(+1) SST, and *f* summer(0) surface zonal wind anomalies correlated with the boreal winter(0) VMI. Areas with correlation significant at the 0.05 level are shaded



results show that the initial warming induced by the SPQ is located in the South American coastal region (Fig. 12a), which extends northwestward toward the central–eastern tropical Pacific through the positive WES feedback mechanism and reduces the mean upwelling cooling there, thereby possibly creating more favorable conditions for establishing a conventional El Niño in the tropical Pacific.

Figure 12e, f show the boreal summer (MJJA-averaged) surface zonal wind related to the previous boreal winter (DJFMA-averaged) SPQ and VM. The figures indicate that there are substantial differences between their related summer surface zonal winds in the tropical Pacific. The anomalous westerly related to the SPQ extends farther east than that related to the VM; the former extends from the western equatorial Pacific to near 130°W, while the latter is confined to west of 150°W. In addition, significant easterly anomalies are seen to be related to the VM in the eastern

equatorial Pacific east of 150°W, while easterly anomalies related to the SPQ are not evident in the eastern equatorial Pacific east of 130°W. The anomalous zonal wind pattern related to the VM is very likely to cause a strong convergence in the central equatorial Pacific, consistent with the findings of DLTS. These results suggest that SSTA patterns associated with the SPQ and VM tend to induce different surface zonal wind patterns in the tropical Pacific, which possibly trigger different ocean–atmosphere feedback processes in the tropical Pacific and finally lead to different types of El Niño events. Kao and Yu (2009) reported that the CPW El Niño appears less related to thermocline variations and may be influenced more by atmospheric forcing, which differ from the conventional El Niño that is associated with basin-wide thermocline and surface wind variations. The analysis presented here only shows a preliminary result of the difference between surface zonal wind in the

tropical Pacific induced by the SPQ and VM; further study is necessary to perform a concrete analysis of the ocean–atmosphere feedback processes that act to develop the initial warming in the tropical Pacific triggered by the VM and SPQ respectively to the CPW and conventional El Niño patterns.

The Niño3.4 index [defined as SST averaged over (170°–120°W, 5°S–5°N)] describes the SST variability in the central equatorial Pacific and is widely used to identify ENSO events. Trenberth and Stepaniak (2001) suggested that the Niño3.4 index is able to represent the general temperature variations in the equatorial Pacific. Kao and Yu (2009) reported that the Niño3.4 index is related to indices of both CPW and conventional El Niño events, although it is not able to separate them. To make a comparison of the relative contribution of the SPQ and VM to ENSO, we selected the Niño3.4 index instead of the CTI (which mainly describes the SST variability in the central and eastern Pacific near the equator) to examine its relationships with the SPQ and VM, respectively. Figure 13a shows the time series of the boreal winter(0) (DJFMA-averaged) VM and SPQ indices overlaid with the boreal winter(+1) (ONDJF-averaged) Niño3.4 index. The correlation between the winter(0) SPQ and the winter(+1) Niño3.4 index reaches 0.52 (significant at the 0.001 level) for the period 1950–2010, which is comparable to (but slightly higher than) the correlation ($R = 0.47$, significant at the 0.001 level) between the boreal winter(0) VM and the boreal winter(+1) Niño3.4 index. This suggests that the SPQ may play an important role in triggering ENSO events that is comparable to that of the VM.

We note that the correlation between the boreal winter(0) SPQ and VM indices time series in Fig. 13a is weak (<0.20). Figure 8c shows that when the SPQ signal peaks during JFM(0) in the South Pacific, there is no marked VM signal observed in the North Pacific, consistent with Fig. 12a. Figure 12b also shows that there is no marked SPQ signal in the South Pacific that is related to the VM. These results indicate that the SPQ event is relatively independent of the VM event. From this starting point, we developed an empirical prediction model of the boreal winter(+1) Niño3.4 index (denoted as WIN(+1)_NINO3.4) using a linear regression method based on both the boreal winter(0) SPQ and VM indices (denoted as WIN(0)_SPQ and WIN(0)_VM, respectively):

$$WIN(+1)_{NINO3.4}(t) = \alpha * WIN(0)_{SPQ}(t) + \beta * WIN(0)_{VM}(t), \quad (3)$$

where t is time in years, and the time series of WIN(0)_SPQ(t), WIN(0)_VM(t), and WIN(+1)_NINO3.4(t), have been standardized. The parameters $\alpha = 0.45$ and $\beta = 0.39$ were obtained by a least-squares fit to the observed WIN(0)_SPQ(t) and WIN(0)_VM(t), respectively, and are significantly

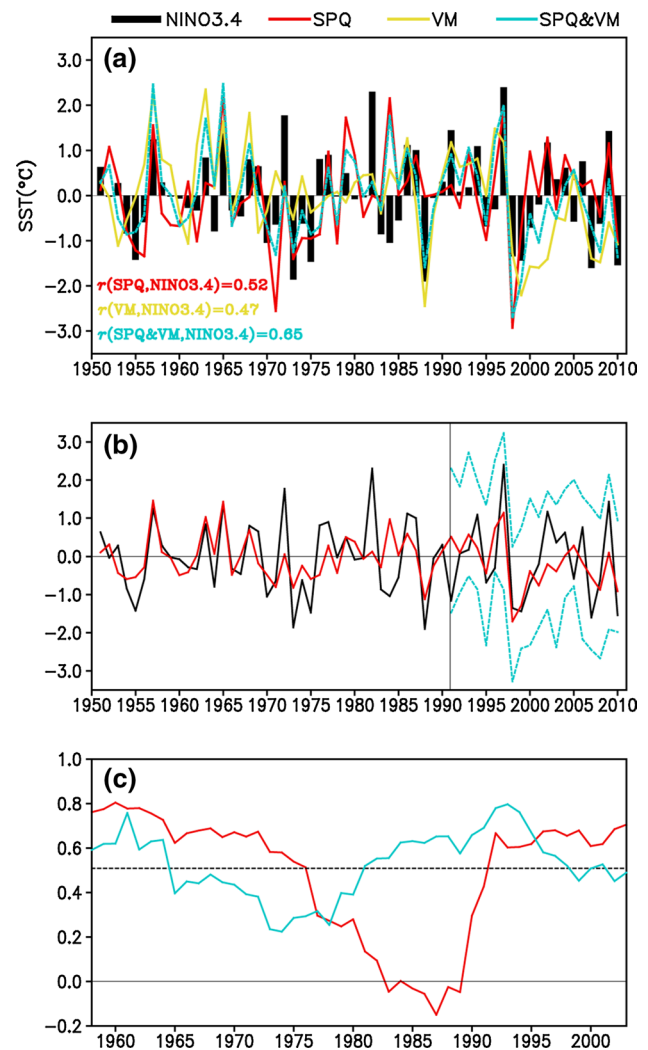


Fig. 13 **a** Time series of the boreal winter(0) SPQ (red line) and VM (yellow line) indices, and the hindcast boreal winter(+1) Niño3.4 index (dashed green line) generated by empirical model (3) using both the boreal winter(0) SPQI and VMI overlaid with the observed boreal winter(+1) Niño3.4 index (black bars). All indices are standardized, and the correlations between various time series are given in the lower left corner. **b** Time series of the observed (black line) and hindcast (red line) boreal winter(+1) Niño3.4 index in the training period (1951–1990) and test period (1991–2010). Blue dashed lines denote the 95 % confidence levels. **c** Time series of the sliding correlations of the boreal winter(0) SPQ (red line) and VM (green line) indices with the boreal winter(+1) Niño3.4 index calculated within a 15-year window that moves year by year through the 1950–2010 period. The horizontal dashed line shows the 0.01 significance level

different from 0 at the 0.05 level. Model (3), which uses both the boreal winter(0) SPQ and VM indices to hindcast the boreal winter(+1) Niño3.4 index, yields a correlation skill of 0.65, which is higher than using only the boreal winter(0) SPQ or VM to forecast the boreal winter(+1) Niño3.4 index. To test the robustness of model (3), the performance of the model was verified for a test period (1991–2010) that was independent of the training period (1951–1990) (Fig. 13b).

The correlation coefficient and root-mean-square-error (RMSE) between the observed and hindcast Niño3.4 index were 0.60 and 0.75 °C in the training period and 0.63 and 0.85 °C in the test period, indicating that the model, even for the independent verification period, is capable of providing a relatively realistic representation of observations.

However, despite the robustness of model (3) in the training and test periods, we notice from Fig. 13a that the relationships between the SPQ and Niño3.4 indices, and between the VM and Niño3.4 indices, show decadal variations. To validate the evolution of their relationships, we show the sliding correlations between the boreal winter(0) SPQI and the boreal winter(+1) Niño3.4 index, and between the boreal winter(0) VMI and the boreal winter(+1) Niño3.4 index, respectively (Fig. 13c). It shows that the correlation between the VM and Niño3.4 indices strengthens from the early 1980s to the mid-1990s, followed by an obvious weakening after the late 1990s. In contrast, the correlation between the SPQ and Niño3.4 indices is very weak in the 1980s, but increases after the early 1990s, and exceeds the correlation between the VM and Niño3.4 indices after the late 1990s. This result shows that the SPQ possibly plays an important role in initiating ENSO events comparable with the VM after the late 1990s. Therefore, to improve the prediction of ENSO, we should not only pay attention to atmospheric and SST signals in the extratropical North Pacific that precede ENSO, but also put greater emphasis on those in the extratropical South Pacific that precede ENSO. The mechanism responsible for the decadal variability of the relationship between the SPQ and ENSO remains unexplained. Wang et al. (2013) suggested that greenhouse gases may play an important role in the decadal variability of the relationship between the western North Pacific (WNP) precursors and ENSO. Further research is required to perform a concrete analysis of the influence of the global warming on the SPQ–ENSO relationship. The roles of the interdecadal Pacific oscillation (IPO) and other internal atmospheric processes in modulating the SPQ–ENSO relationship should be taken into account as well.

6 Summary and discussion

This study establishes the existence of a marked wave train structure of SLP anomalies from the mid-latitude South Pacific to Argentina that precedes ENSO by 1 year. This wave train structure of SLP anomalies over the South Pacific resembles the PSA pattern. The PSA can force a quadrupole SST pattern in the South Pacific via changes in the net surface heat flux. This South Pacific quadrupole SST pattern induced by the PSA is referred to as the SPQ. It was found that the SPQ and ENSO are most closely

correlated when the SPQ leads ENSO by 9 months. In contrast to the PSA, the SPQ and ENSO exhibit maximum correlation with a larger value, indicating that the SPQ, as an ocean bridge (or conduit) connecting the PSA and ENSO, may serve as a better precursor for ENSO events than the PSA.

The present analysis suggests that the following dynamical mechanism links the PSA, SPQ, and ENSO at the seasonal timescale. The PSA-like extratropical SLP variability during austral summer forces a quadrupole SST pattern in the South Pacific (i.e., the SPQ). The SPQ (mainly its related negative SSTAs off the east coast of Australia) may extend northwestward toward the north coast of Australia through a positive WES feedback, which can lead to the anomalous westerlies along the equator that contribute to the development of ENSO. In addition, the warming along the west coast of South America associated with the SPQ may extend northwestward toward the central–eastern equatorial Pacific through a positive WES feedback. The warming in the central–eastern equatorial Pacific then intensifies the zonal wind anomalies along the equator. ENSO develops in phase with the zonal wind anomalies along the equator during the following austral winter, and peaks during the following austral summer, about 9 months after the peak in the SPQ. These phase relationships among the PSA, SPQ, zonal wind anomalies along the equator, and ENSO are consistent with the so-called SFM hypothesis: the PSA imparts an SST footprint (i.e., the SPQ) onto the ocean during austral summer; the SST footprint subsequently forces the zonal wind anomalies along the equator that ultimately result in ENSO events during the following austral summer via ocean–atmosphere coupling in the tropics.

Previous studies have emphasized the role of North Pacific extratropical forcing in ENSO variability, but paid little attention to the independent contribution of South Pacific extratropical forcing to the initiation of ENSO events. The present study demonstrates that South Pacific extratropical forcing (i.e., the PSA/SPQ) is relatively independent of North Pacific extratropical forcing (i.e., the NPO/VM). They may, either separately or together, influence the occurrence of ENSO events, and the importance of the PSA/SPQ in initiating ENSO events is comparable with that of the NPO/VM. The NPO/VM and PSA/SPQ appear to have different relationships with different types of El Niño. The NPO/VM tends to be more closely linked to the CPW El Niño than to the conventional El Niño, while the PSA/SPQ tends to be more closely linked to the conventional El Niño than to the CPW El Niño.

The relative independence of the VM and SPQ leads us to speculate that the VM and SPQ variations may together serve as a precursor for ENSO events. Therefore, we established an empirical model to predict the Niño3.4 index in the following boreal winter using both the boreal winter

SPQ and VM indices. A hindcast performed for the period 1950–2010 produced skillful forecasts of the Niño3.4 index with a leading time of up to 1 year. As the SPQ and VM indices can be easily obtained in real time before the peak of ENSO, this empirical model can be used for the practical forecasting of ENSO.

Previous studies reported two subtropical–tropical coupled patterns that are both significantly correlated to ENSO with lead times of up to 6–12 months: the North Pacific meridional mode (NPMM) with its subtropical center of action located in the northeast Pacific (Chiang and Vimont 2004; Chang et al. 2007; Zhang et al. 2009a, b), and the South Pacific meridional mode (SPMM) with its subtropical center of action located in the southeast Pacific (Zhang et al. 2014a, b). These studies present both observational and modeling evidence for the importance of the PMM patterns in initiating ENSO events. DLTS report that the VM in the extratropical North Pacific is closely linked to the NPMM. From Figs. 8c and 12a, it is apparent that the SSTA signature of the SPQ in the South Pacific bears a resemblance to the SPMM pattern. The correlation of the monthly SPQI with the monthly SPMM index [defined as the area-mean SSTAs over 110°–90°W, 15°–25°S] reaches 0.44 (significant at the 0.001 level). These results suggest that analogous to the North Pacific climate patterns (i.e., the VM and NPMM), the South Pacific climate patterns (i.e., the extratropical SPQ and subtropical SPMM) are also strongly interconnected during the development of ENSO. In addition, it is noteworthy that Zhang et al. (2014a), based on evidence from both observations and models, reported that the SPMM and the NPMM seem to be related to different ENSO flavors: the equatorial signature of the SPMM resembles the canonical El Niño while that associated with the NPMM is more like the CPW El Niño. Their findings are consistent with our argument that the South and North Pacific extratropical variability can trigger different types of ENSO events. However, further study based on simulations in fully coupled ocean–atmosphere models is needed to understand the mechanism by which the South and North Pacific extratropical forcings influence ENSO.

Acknowledgments This research was jointly supported by the 973 project of China (2012CB955200), the National Natural Science Foundation of China (41175069), the China Special Fund for Meteorological Research in the Public Interest (GYHY201306031), and the Strategic Priority Research Program of the Chinese Academy of Sciences (XDA11010303).

References

- Alexander MA, Vimont DJ, Chang P, Scott JD (2010) The impact of extratropical atmospheric variability on ENSO: testing the seasonal footprinting mechanism using coupled model experiments. *J Clim* 23:2885–2901
- Ashok K, Behera SK, Rao SA, Weng H, Yamagata T (2007) El Niño Modoki and its possible teleconnection. *J Geophys Res* 112:C11007. doi:10.1029/2006JC003798
- Ballester J, Rodríguez-Arias MÀ, Rodó X (2011) A new extratropical tracer describing the role of the western Pacific in the onset of El Niño: implications for ENSO understanding and forecasting. *J Clim* 24:1425–1437
- Bond NA, Overland JE, Spillane M, Stabeno P (2003) Recent shifts in the state of the North Pacific. *Geophys Res Lett* 30:2183. doi:10.1029/2003GL018597
- Bretherton CS, Smith C, Wallace JM (1992) An intercomparison of methods for finding coupled patterns in climate data. *J Clim* 5:541–560
- Carril AF, Navarra A (2001) Low-frequency variability of the Antarctic circumpolar wave. *Geophys Res Lett* 28:4623–4626
- Carton JA, Giese BS (2008) A reanalysis of ocean climate using Simple Ocean Data Assimilation (SODA). *Mon Wea Rev* 136:2999–3017
- Chang P, Zhang L, Saravanan R, Vimont DJ, Chiang JCH, Ji L, Seidel H, Tippet MK (2007) Pacific meridional mode and El Niño–Southern Oscillation. *Geophys Res Lett* 34:L16608. doi:10.1029/2007GL030302
- Chiang J, Vimont D (2004) Analogous Pacific and Atlantic meridional modes of tropical atmosphere–ocean variability. *J Clim* 17:4143–4158
- Ding QH, Steig EJ, Battisti DS, Wallace JM (2012) Influence of the tropics on the southern annular mode. *J Clim* 25:6330–6348
- Fogt R, Bromwich D (2006) Decadal variability of the ENSO teleconnection to the high-latitude South Pacific governed by coupling with the southern annular mode. *J Clim* 19:979–997
- Gong DY, Wang SW (1999) Definition of Antarctic oscillation index. *Geophys Res Lett* 26:459–462
- Grassi B, Redaelli G, Visconti G (2005) Simulation of Polar Antarctic trends: influence of tropical SST. *Geophys Res Lett* 32:L23806. doi:10.1029/2005GL023804
- Harrison DE, Larkin NK (1998) El Niño–Southern Oscillation sea surface temperature and wind anomalies, 1946–1993. *Rev Geophys* 36:353–400
- Holbrook NJ, Bindoff NL (1997) Interannual and decadal temperature variability in the southwest Pacific Ocean between 1955 and 1988. *J Clim* 10:1035–1049
- Jin FF, An SI (1999) Thermocline and zonal advection feedbacks within the equatorial ocean recharge oscillator model for ENSO. *Geophys Res Lett* 26:2989–2992
- Jin D, Kirtman BP (2009) Why the Southern Hemisphere ENSO responses lead ENSO? *J Geophys Res* 114:D23101. doi:10.1029/2009JD012657
- Kalnay E et al (1996) The NCEP–NCAR 40-Year Reanalysis Project. *Bull Am Meteor Soc* 77:437–471
- Kao HY, Yu JY (2009) Contrasting eastern Pacific and central Pacific types of ENSO. *J Clim* 22:615–632
- Karoly DJ (1989) Southern Hemisphere circulation features associated with El Niño–Southern Oscillation events. *J Clim* 2:1239–1252
- Kidson JW, Renwick JA (2002) The southern hemisphere evolution of ENSO during 1981–99. *J Clim* 15:847–863
- Kug JS, Jin FF, An SI (2009) Two types of El Niño events: cold tongue El Niño and warm pool El Niño. *J Clim* 22:1499–1515
- Kwok R, Comiso JC (2002) Southern ocean climate and sea ice anomalies associated with the southern oscillation. *J Clim* 15:487–501
- L’Heureux ML, Thompson DWJ (2006) Observed relationships between the El Niño—Southern Oscillation and the extratropical zonal-mean circulation. *J Clim* 19:276–287
- Larkin NK, Harrison DE (2005) Global seasonal temperature and precipitation anomalies during El Niño autumn and winter. *Geophys Res Lett* 32:L16705. doi:10.1029/2005GL022860

- Li Y, Li JP, Feng J (2012) A teleconnection between the reduction of rainfall in southwest Western Australia and north China. *J Clim* 25:8444–8461
- Li G, Li CY, Tan YK, Pan J (2013a) Impacts of the central and eastern Pacific types of ENSO on sea surface temperature in the South Pacific. *Theor Appl Climatol* 114:315–327
- Li XF, Yu JJ, Li Y (2013b) Recent summer rainfall increase and surface cooling over Northern Australia: a response to warming in the tropical Western Pacific. *J Clim* 26:7221–7239
- Mo KC (2000) Relationships between low-frequency variability in the Southern Hemisphere and sea surface temperature anomalies. *J Clim* 13:3599–3610
- Mo KC, Higgins RW (1998) The Pacific–South American modes and tropical convection during the Southern Hemisphere winter. *Mon Wea Rev* 126:1581–1596
- Montegut CD, Madec G, Fischer AS, Lazar A, Iudicone D (2004) Mixed layer depth over the global ocean: an examination of profile data and a profile-base climatology. *J Geophys Res Oceans* 109:C12003. doi:[10.1029/2004JC002378](https://doi.org/10.1029/2004JC002378)
- Newman M, Compo GP, Alexander MA (2003) ENSO-forced variability of the Pacific decadal oscillation. *J Clim* 16:3853–3857
- North GR, Bell TL, Cahalan RF, Moeng FJ (1982) Sampling errors in the estimation of empirical orthogonal function. *Mon Wea Rev* 110:699–706
- Picaut J, Masia F, du Penhoat Y (1997) An advective-reflective conceptual model for the oscillatory nature of the ENSO. *Science* 277:663–666
- Pyper BJ, Peterman RM (1998) Comparison of methods to account for autocorrelation in correlation analyses of fish data. *Can J Fish Aquat Sci* 55:2127–2140
- Rayner NA, Brohan P, Parker DE, Folland CK, Kennedy JJ, Vanicek M, Ansell T, Tett SFB (2006) Improved analyses of changes and uncertainties in sea surface temperature measured in situ since the mid-nineteenth century: the HadSST2 dataset. *J Clim* 19:446–469
- Ribera P, Mann ME (2003) ENSO related variability in the Southern Hemisphere, 1948–2000. *Geophys Res Lett* 30:1006. doi:[10.1029/2002GL015818](https://doi.org/10.1029/2002GL015818)
- Rogers JC (1981) The North Pacific oscillation. *J Climatol* 1:39–57
- Schneider N, Cornuelle B (2005) The forcing of the Pacific decadal oscillation. *J Clim* 18:4355–4373
- Simmonds I, Jacka TH (1995) Relationships between the interannual variability of Antarctic sea-ice and the Southern Oscillation. *J Clim* 8:637–647
- Terray P (2011) Southern Hemisphere extra-tropical forcing: a new paradigm for El Niño—Southern Oscillation. *Clim Dyn* 36:2171–2199
- Thompson DWJ, Wallace JM (2000) Annular modes in the extra-tropical circulation. Part I: month-to-month variability. *J Clim* 13:1000–1016
- Toniazzo T (2010) Climate variability in the south-eastern tropical Pacific and its relation with ENSO: a GCM study. *Clim Dyn* 34:1093–1114
- Trenberth KE, Stepaniak DP (2001) Indices of El Niño evolution. *J Clim* 14:1697–1701
- Vimont DJ, Battisti DS, Hirst AC (2001) Footprinting: a seasonal connection between the tropics and mid-latitudes. *Geophys Res Lett* 28:3923–3926
- Vimont DJ, Wallace JM, Battisti DS (2003a) The seasonal footprinting mechanism in the Pacific: implications for ENSO. *J Clim* 16:2668–2675
- Vimont DJ, Battisti DS, Hirst AC (2003b) The seasonal footprinting mechanism in the CSIRO general circulation models. *J Clim* 16:2653–2667
- Walker GT, Bliss EW (1932) World weather V. *Mem Roy Meteor Soc* 4:53–84
- Wang SY, L’Heureux M, Yoon JH (2013) Are greenhouse gases changing ENSO precursors in the western North Pacific? *J Clim* 26:6309–6322
- White WB, Annis J (2004) Influence of the Antarctic circumpolar wave on El Niño and its multidecadal changes from 1950 to 2001. *J Geophys Res* 109: doi:[10.1029/2002jc001666](https://doi.org/10.1029/2002jc001666)
- White WB, Peterson RG (1996) An Antarctic circumpolar wave in surface pressure, wind, temperature and sea-ice extent. *Nature* 380:699–702
- Xie SP, Philander SGH (1994) A coupled ocean–atmosphere model of relevance to the ITCZ in the eastern Pacific. *Tellus* 46A:340–350
- Yu JY, Kim ST (2011) Relationships between extratropical sea level pressure variations and the central Pacific and eastern Pacific types of ENSO. *J Clim* 24:708–720
- Yuan XJ, Martinson DG (2000) Antarctic sea ice extent variability and its global connectivity. *J Clim* 13:1697–1717
- Zhang L, Chang P, Ji L (2009a) Linking the Pacific meridional mode to ENSO: coupled model analysis. *J Clim* 22:3488–3505
- Zhang L, Chang P, Tippett MK (2009b) Linking the Pacific meridional mode to ENSO: utilization of a noise filter. *J Clim* 22:905–922
- Zhang HH, Clement A, Di Nezio P (2014a) The South Pacific meridional mode: a mechanism for ENSO-like variability. *J Clim* 27:769–783
- Zhang HH, Deser C, Clement A, Tomas R (2014b) Equatorial signatures of the Pacific Meridional Modes: dependence on mean climate state. *Geophys Res Lett* 41:2. doi:[10.1002/2013GL058842](https://doi.org/10.1002/2013GL058842)